JOURNAL OF SPACECRAFT AND ROCKETS
Vol. 47, No. 4, July–August 2010

Computational Fluid Dynamics Methods for Hypersonic Flow Around Blunted-Cone–Cylinder–Flare

Shiroshana Tissera and Dimitris Drikakis*
Cranfield University, Cranfield, England MK43 0AL, United Kingdom
and
Trevor Birch
Defence Science and Technology Laboratory,
Porton Down, Salisbury, England SP4 OJQ, United Kingdom

DOI: 10.2514/1.46722

This paper presents an investigation of numerical schemes for the hypersonic flow around a blunted-cone–cylinder–flare (HB-2). The investigation is based on a finite volume computational fluid dynamics code using the Harten–Lax–van Leer–contact Riemann solver in conjunction with four numerical reconstruction schemes with order of accuracy ranging from second–ninth order. Comparisons are presented with experimental data for the pressure and heat transfer. The results show that very-high-order schemes such as weighted essentially nonoscillatory fifth- and ninth-order methods may provide slightly better results for freestream Mach numbers less than 10; however, there are no obvious benefits over second-order methods for Mach numbers greater than 10.

Introduction

IN A recent study [1] a series of computations performed by researchers in the United States and Europe were presented for two generic configurations, double-cone and cylinder, and compared with experimental data. For low-enthalpy flows it was shown that the predicted heat transfer and surface pressure are in good agreement with the experiment. Interestingly, all simulations also predicted a unsteady flow for the low-enthalpy double-cone configuration in direct contrast to the experiment. The above investigation prompts the need for further study of numerical methods for other hypersonic configurations.

One hypersonic configuration that has attracted interest in the past is the blunted-cone–cylinder–flare designated as HB-2 test case [2–8] (Fig. 1). Experiments have been carried out in various wind tunnels such as the von Kármán Gas Dynamics Facility (VKF), the Arnold Engineering Development Center, and ONERA to measure quantities such as pressure and heat transfer on the wall with varying Mach numbers and angle of attacks. A limited number of computational studies has also been presented in the literature [9,10]; however, an assessment of different high-order methods versus second order of accuracy has not yet been fully explored.

Numerical reconstruction is a common approach to extend the order of accuracy beyond first-order. It is usually provided via the second-order MUSCL [11], but there have also been higher-order extensions of the MUSCL scheme up to fifth order [12]. Another approach to construct high-order methods is provided by the essentially nonoscillatory (ENO) method [13]. Third-order ENO schemes were used by [14] to study the effects of shockwave–freestream interactions of transient hypersonic flow. The ENO methods have not found widespread use, partly because they were quickly superseded by the weighted ENO (WENO) schemes [15]. Fifth-order WENO schemes have been employed to study the boundary layer over a blunt cone [16–19]. These studies included variants of the WENO scheme such as a preconditioned (P-WENO) scheme for solving the Navier–Stokes equations consisting of a first-order component in conjunction with the preconditioned Roe solver and a third-order component based on a preconditioned WENO scheme.

The standard WENO reconstruction of Jiang and Shu [15] (WENO-JS) has been successfully applied to many problems featuring discontinuities [20–23]. There have also been efforts to improve the efficiency and robustness of the original WENO scheme. Henrick et al. [24] introduced the mapped WENO (WENO-M) scheme that was capable of achieving optimal order of accuracy near critical points. More recently, Borges et al. [25] presented a new WENO scheme (WENO-Z) by implementing higher-order smoothness indicators with a new set of nonoscillatory weights that gives less dissipation and higher resolution than the original WENO-JS scheme. The results obtained for the fifth-order reconstruction for this scheme are as sharp as those obtained using the mapped WENO (WENO-M) scheme with the computational cost being lower when the mapping is not performed.

The aim of the study is to present our experience in relation to a range of schemes for the HB-2 configuration. The study includes the fifth- and ninth-order WENO-M schemes as well as the second- and fifth-order MUSCL schemes. Comparisons are performed against experimental data for the wall pressure and heat transfer distributions. The flow solvers used in the study are not new; however, to our knowledge, it is the first time that several numerical reconstruction schemes have been tested for a range of Mach numbers for the HB-2 geometry.

Numerical Method

The computational study is based on the computational fluid dynamics code CNS3D developed in [26–30]. The code uses the HLLC Riemann solver [31]. The HLLC Riemann solvers assumes a three-wave structure of the Riemann problem solution, allowing for two intermediate states enclosed by the two fastest waves. The HLLC Riemann solver does not use linearization of the equations and works well for low-density problems and sonic points without any fixes. It has been successfully been used to simulate a variety of flow [29,32]. The Euler equations in axisymmetric formulation are solved by an implicit unfactored scheme that uses Newton iterations and Gauss–Seidel relaxation techniques [33,34].

Two families of numerical reconstruction have been employed in this study: 1) second- and fifth-order variants of the MUSCL schemes and 2) fifth- and ninth-order WENO schemes. These schemes are briefly described below.

Received 13 August 2009; revision received 27 April 2010; accepted for publication 28 April 2010.

*Professor, Fluid Mechanics and Computational Science; d.drikakis@cranfield.ac.uk. Life Senior Member AIAA (Corresponding Author).

Table 1 Flow conditions for the HB-2 hypersonic configuration

Case	1	2	3	4
M_∞	17.8	9.59	7.5	5.0
Re/m	0.02×10^6	2.1×10^6	0.13×10^6	2.32×10^6
P_∞, Pa	29.5	75	210	3748
ρ_∞, Kgm^{-3}	3.95×10^{-4}	5.0×10^{-3}	9.1×10^{-3}	5.1×10^{-3}
T_∞, K	287	52	138.9	138.9

Table 2 Availability of experimental data with reference to wall pressure and heat flux

Case	Pressure	Heat flux
1	✓	✓
2	——	✓
3	✓	——
4	✓	——

The MUSCL scheme uses piecewise linear spatial reconstruction that is either second-order-accurate [11] or fifth-order-accurate [12] in smooth regions of the flow away from extrema. To control oscillations, slope limiters are used to keep the interpolation within an acceptable range, thereby ensuring a total-variation-diminishing (TVD) condition. This reconstruction procedure typically uses piecewise linear representation of data and the boundary extrapolated values at the interface position between cells i and $i+1$ can be represented as

$$U_L = U_i + \frac{1}{4}\left[(1-k)\varphi(r_L)(U_i - U_{i-1}) + (1+k)\varphi\left(\frac{1}{r_L}\right)(U_{i+1} - U_i)\right] \tag{1}$$

$$U_R = U_{i+1} + \frac{1}{4}\left[(1-k)\varphi(r_R)(U_{i+2} - U_{i+1}) + (1+k)\varphi\left(\frac{1}{r_R}\right)(U_{i+1} - U_i)\right] \tag{2}$$

where φ is the slope-limiter function, and k is a free parameter that is usually set to one-third for the third-order scheme. The ratios of upwind to downwind changes of the flow variables r_L and r_R are defined as

$$r_L = \frac{U_{i+1} - U_i}{U_i - U_{i-1}}, \qquad r_r = \frac{U_{i+1} - U_i}{U_{i+2} - U_{i+1}}$$

A review of limiter functions can be found in [31,34]. In the present work, the limiters of van Leer [11] and Drikakis (as reported in [26,27,29,30]) labeled as VL and DD, respectively, are used.

All of the above limiters switch to zero at local maxima and minima, and so the resulting total-variation-diminishing (TVD) methods are only first-order-accurate in the maximum norm. This is not a desirable property, which can result in increased numerical errors in the smooth part of the flow.

An improvement over TVD methods comes with the ENO and WENO schemes. These methods combine a very high order of spatial accuracy when the solution is smooth and at the same time do not produce spurious oscillations near sharp gradients or across discontinuities. Unlike MUSCL reconstruction, the WENO reconstruction considers several candidate stencils for obtaining high-order boundary extrapolated data. The values of the flow variables from each stencil are combined using the nonlinear solution adaptive weights, which depend on the smoothness of each candidate stencil. As a result, the discontinuous stencils are assigned a very low weight.

In particular, the use of three stencils each consisting of three cells can theoretically produce a fifth-order-accurate reconstruction. The weights are made dependent on the smoothness of each candidate stencil: those stencils adjudged to contain a discontinuity are given a very small weight. This can be expressed as

$$U_{j+\frac{1}{2}} = \sum_{m=0}^{2} \omega_m \hat{U}^m_{j+\frac{1}{2}} \tag{3}$$

where $\hat{U}^m_{j+\frac{1}{2}}$ is the extrapolated value for each stencil, and ω_m is the weight corresponding to stencil m. Jiang and Shu [15] provide the following expression for the weights:

$$\omega_m = \frac{\alpha_m}{\sum_{l=0}^{2} \alpha_l} \tag{4}$$

where

$$\alpha_m = \frac{\bar{\omega}_m}{(\varepsilon + \beta_m)^p}$$

where ε is a small parameter to keep α bounded, β_m are the smoothness indicators as laid out in [15,20,22], p is a free parameter, and $\bar{\omega}_m$ are the ideal (so-called linear) weights required to achieve the fifth-order-accurate upwind scheme in smooth flow.

More recent work [24] has shown that the above formulation is not sufficient to maintain the maximum possible accuracy around critical points. They suggest that a simple mapping of the weights calculated as before to bring them closer to the ideal weights, while still retaining the required behavior away from these regions, resolves this issue. The modified weights are calculated as

$$\omega_m^{(M)} = \frac{\alpha_m^*}{\sum_{i=0}^{2} \alpha_m^*} \tag{5}$$

$$\alpha_m^* = g_m(\omega_m) \tag{6}$$

$$g_m(\omega_m) = \frac{\omega_m(\bar{\omega}_m + \bar{\omega}_m^2 - 3\bar{\omega}_m\omega_m + \omega_m^2)}{\bar{\omega}_m^2 + \omega_m(1 - 2\bar{\omega}_m)} \tag{7}$$

Thus, the mapping is relatively cheap. In implementation it has also been seen to improve the results, gaining greater convergence for a

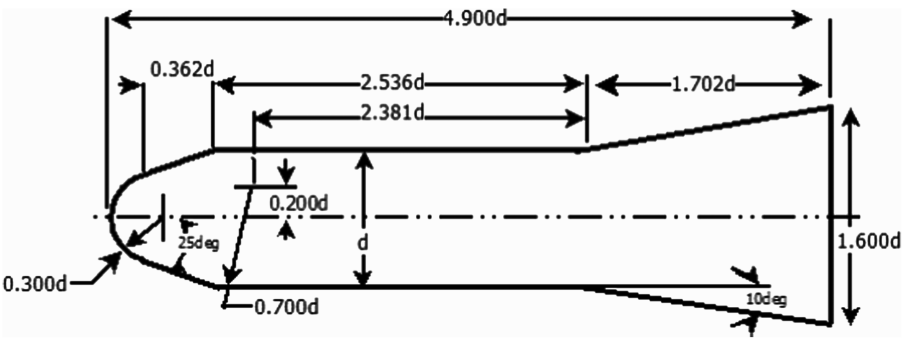

Fig. 1 Schematic of HB-2 geometry.

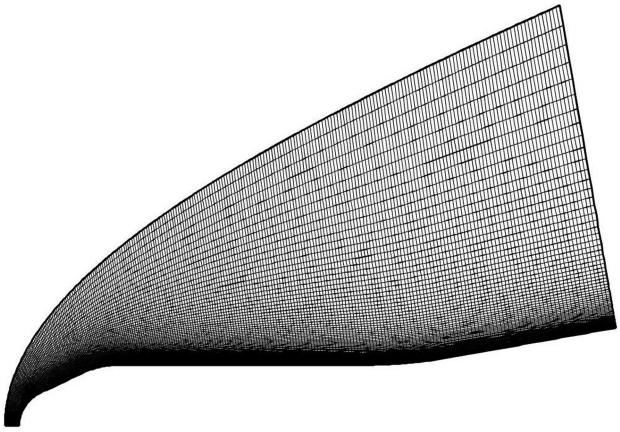

Fig. 2 HB-2 computational grid with clustered cells near the wall.

coarse grid. The extension to ninth order is straightforward building upon a convex combination of five-cell stencils.

Results

Four different cases for the HB-2 configuration have been considered with flow conditions according to Table 1. The availability of experimental data for the wall pressure and heat flux is shown in Table 2. The initial conditions for cases 1 and 2 originate from the experimental data obtained from the VKF and the Japan Aerospace Exploration Agency test facilities, respectively. All cases are simulated at zero angle of attack.

Even though the HB-2 configuration does not give rise to overly complicated flow features, to accurately capture the heat transfer and pressure over the surface, it is important to use a sufficiently refined computational mesh. In the present work, several levels of grid refinement have been adopted to assess the improvements made to the numerical accuracy with the increment in grid resolution and order of reconstruction. A typical grid clustered near the wall is shown in Fig. 2. The boundary conditions are supersonic inflow and outflow, no-slip isothermal surface on the cone surface and symmetry along the cone axis.

The Mach number contours for all cases are shown below and give an insight into the flow field over the test case (see Fig. 3). A strong shock wave is formed upstream of the body with the second one is seen over the cylinder-flare junction. A detailed grid convergence study has been carried out for case 1. The heat transfer to the surface is plotted to examine the improvement in numerical results with the increment in grid density. The results obtained with first-order and higher-order reconstruction methods over all grid resolutions are also compared, see Figs. 4–7.

A sequence of grid resolutions has been used, with 256×128, 128×48, and 98×48 cells, which are referred below as fine, medium, and coarse grids, respectively. Great care has been taken to ensure that cells adjacent to the wall have grid lines perpendicular to it. The results at different grid resolutions are shown for different schemes in Figs. 4–6. The heat transfer to the nose region at the front and flare region at the back is under predicted by all schemes over all grid resolutions. Further investigations are essential to clarify these discrepancies as the front part of the HB-2 flare experiences the highest heat transfer values compared to rest of the body during hypersonic flight. It might also be worthwhile to investigate the problem under chemically reacting gas conditions to see if there is

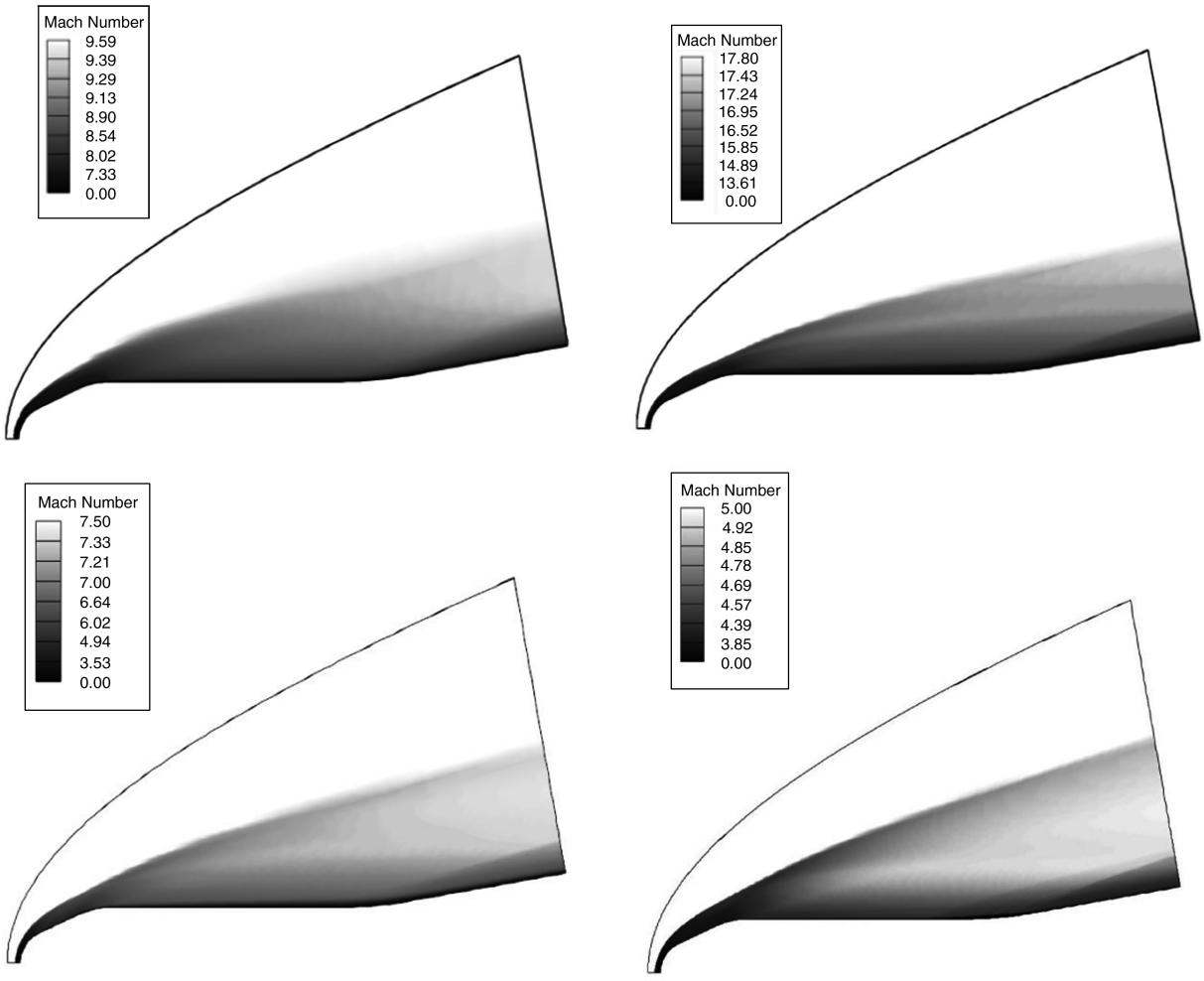

Fig. 3 Mach number contours for cases 1 to 4 (top to bottom and left and to right).

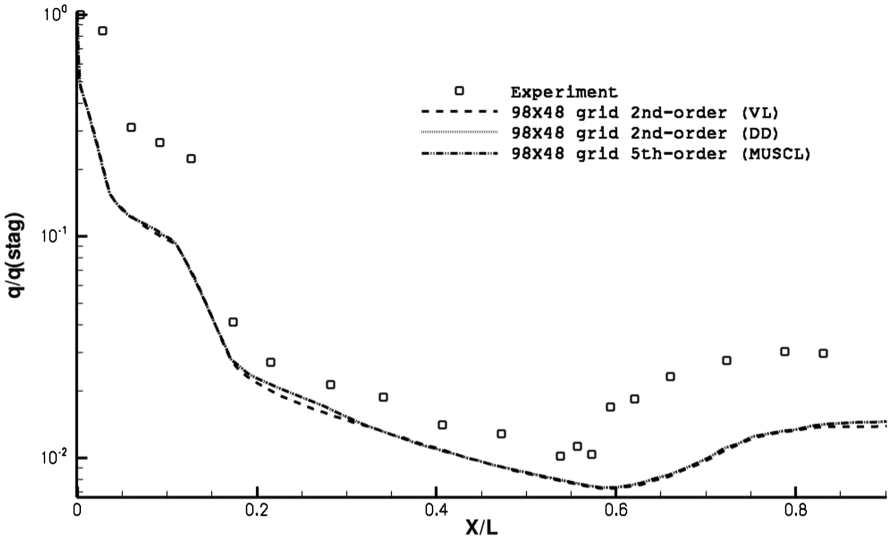

Fig. 4 Heat transfer rate computed on the 96 × 48 grid for case 1. The heat transfer is nondimensionalized with reference to the heat transfer at the stagnation point.

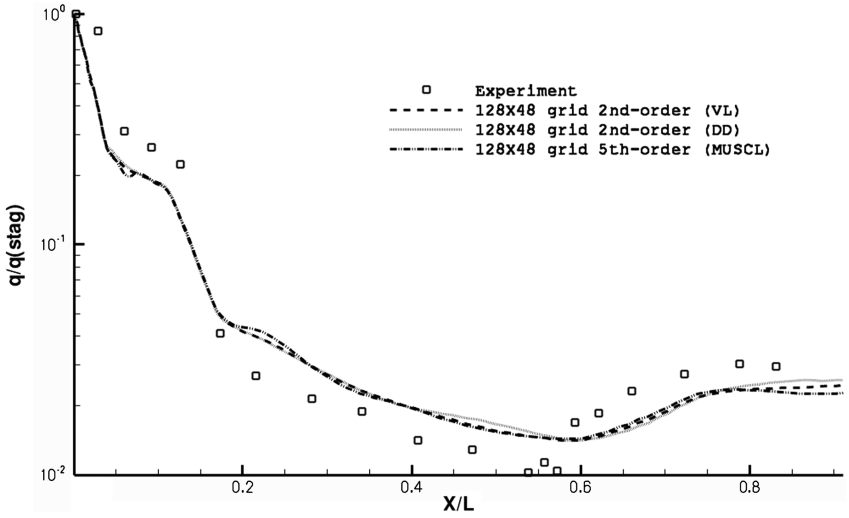

Fig. 5 Heat transfer distribution computed on the 128 × 48 grid for case 1.

any improvement. As the exact details of the enthalpy conditions in the freestream are not clear the comparison with experiment is somewhat difficult.

As expected the grid resolution influences the computational results for all orders of accuracy. The overall agreement between predicted values by all TVD schemes over the cylindrical sections via the use of fine mesh and the experiment is good. The results obtained for the WENO scheme are not presented due to the oscillations present and the WENO scheme does not appear to perform well at such a high Mach number equal to 17.8. It seems as if the design of WENO methods for such demanding applications needs further investigation, which is beyond the scope of the present paper.

As the exact freestream values are not available, the choice of the freestream temperature may affect the comparison with the experimental data. On the other hand, it is possible the discrepancy is within the range of experimental uncertainty and test conditions could be modeled to investigate it further.

Figures 7–9 show the pressure results obtained for the MUSCL second- (two different limiters) and fifth-order reconstruction schemes over all grid resolutions. The overall agreement between the computational results and experimental data is good, with minor discrepancies in the front region of the cylindrical section.

The second-order (DD limiter) MUSCL gives overall the best results for the heat transfer distribution. The schemes give similar results for the wall pressure. The fifth- and ninth-order WENO schemes did not satisfactorily converge for this case; therefore, the results are not included.

The stagnation pressures for the second-order (VL), second-order (DD), and fifth-order MUSCL schemes are very similar and equal to 12.1, 12, and 12 KPa, respectively, while the stagnation heat fluxes are 4050, 4260 and 3750 KW/m^2, respectively. Note that the above values correspond to the values of the first cell off the wall, where in the case of the finite volume methods the values are stored. The experimental stagnation values are not available in the literature.

The heat transfer results for case 2 on the 128×48 and 256×96 grids are shown in Figs. 10 and 11, respectively. The VL and DD limiters gave identical results; thus, only the results with the VL limiter are shown. Moreover, the ninth-order WENO was unstable for this case too without being able to satisfactorily converge.

According to [7], the experimental heat flux stagnation value is 137.62 kW/m^2 (Sec. 4 in the experimental report [7]). The predicted value in this study was found to be 127.2 and 118.5 kW/m^2 for the second- and fifth-order MUSCL schemes, respectively. Similar

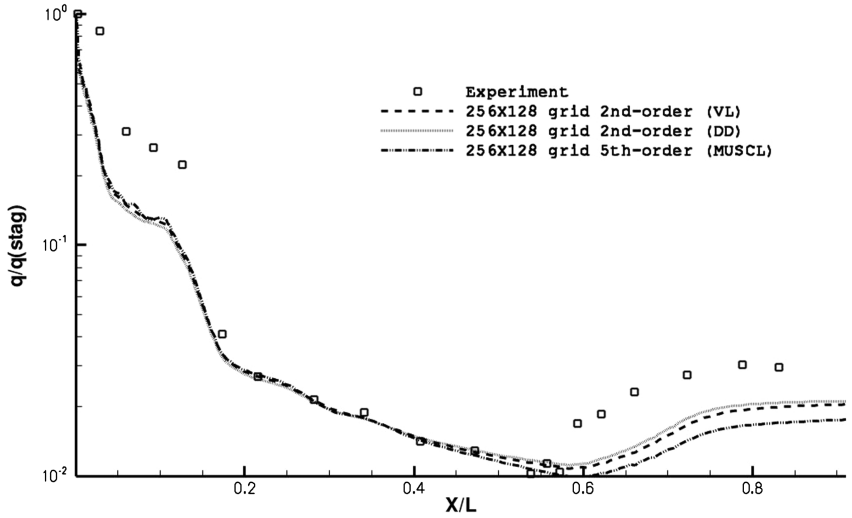

Fig. 6 Heat transfer distribution computed on the 256 × 128 grid for case 1.

to case 1, the stagnation values are computed in the first cell off the wall, which compares better in terms of position with the station 3 of the experiment corresponding to heat flux value of 126.77 kW/m^2. As regard the heat flux stagnation value, the second-order MUSCL agrees better with the experiment than the fifth-order MUSCL scheme. With respect to the dimensionless heat flux distribution, the comparison with the experiment is satisfactory and the fifth-order WENO performs overall better than the second-order MUSCL

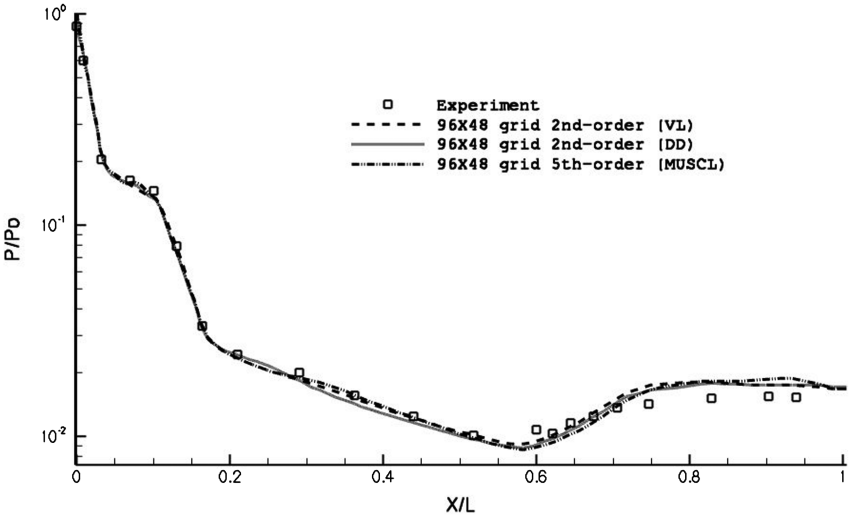

Fig. 7 Pressure distribution computed on the 96 × 48 grid for case 1.

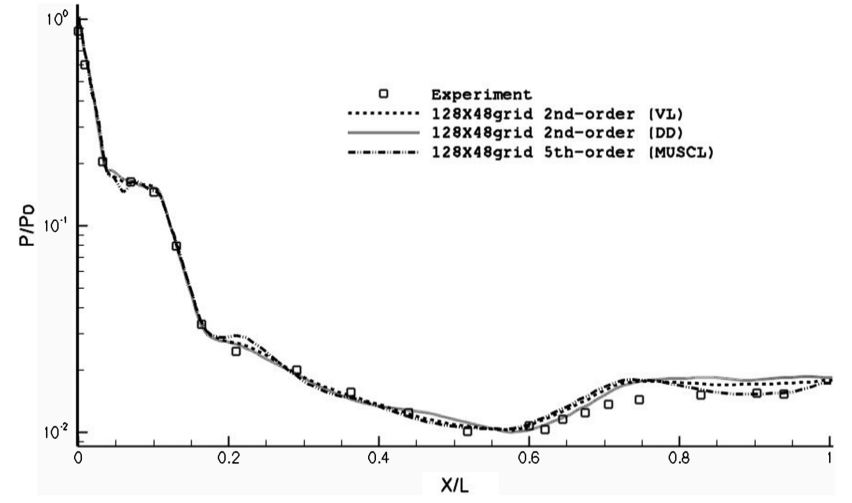

Fig. 8 Pressure distribution computed on the 128 × 48 grid for case 1.

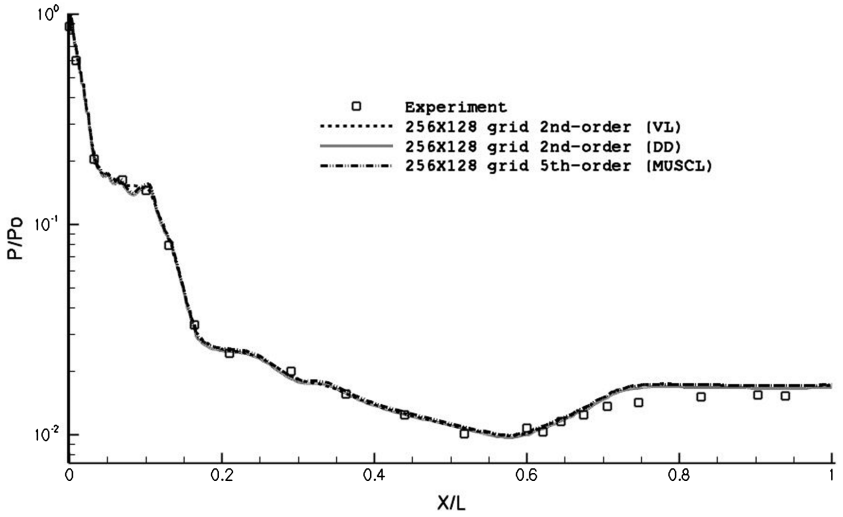

Fig. 9 Pressure distribution computed on the 256 × 128 grid for case 1.

scheme. In comparison to case 1, for this case the heat transfer predictions at the nose and in the flare region are significantly better. Numerical experiments were also performed with the fifth-order MUSCL scheme; however, the scheme resulted in spurious oscillations. When the grid resolution was increased the oscillations were reduced but not completely, thus leading to convergence problems. The second-order MUSCL using the DD limiter gave exactly the same results with the VL limiter; hence, only the results of the VL limiter are presented in Figs. 10 and 11.

For case 3 all methods gave very similar results for the pressure distribution (Fig. 12), including the fifth-order MUSCL, the fifth-order WENO and the second-order MUSCL (DD limiter). For this case, even a first-order scheme gives satisfactory results. Therefore, Fig. 12 presents indicative results from the first-order, second-order MUSCL and ninth-order WENO. The pressure stagnation values for the first-, second-, and ninth-order schemes were computed as 90, 85, and 95 kPa, respectively.

Case 4 is different from the previous cases, because it features separation around the cylinder-flare junction. This is indicated in the pressure distribution by a double-step profile (Figs. 13 and 14). Using first-order of accuracy the separation cannot be captured. The reattachment point is well matched to experiment, although the total separation length is somewhat smaller. The ninth-order WENO captures better the separation point; however, it shifts the reattachment point downstream. The second-order MUSCL gives better results for the reattachment point.

As regard the fifth-order MUSCL and second-order MUSCL (DD limiter), these schemes gave almost identical results with the second-order MUSCL (VL limiter); hence, they are not included in Figs. 13 and 14. Note that past research [27,29,30] has shown that the DD limiter is overall more robust than the VL limiter for a wide range of Mach numbers. For Case 4, the pressure stagnation values for the first-, second-, and ninth-order schemes are 38, 38, and 38.6 kPa, respectively.

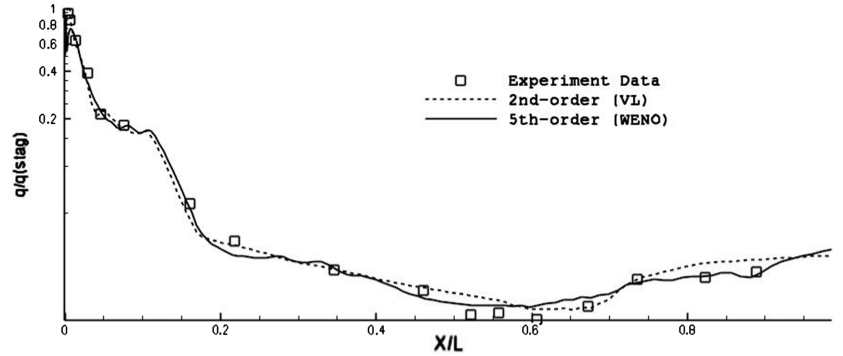

Fig. 10 Heat transfer distribution on the 128 × 48 grid for case 2.

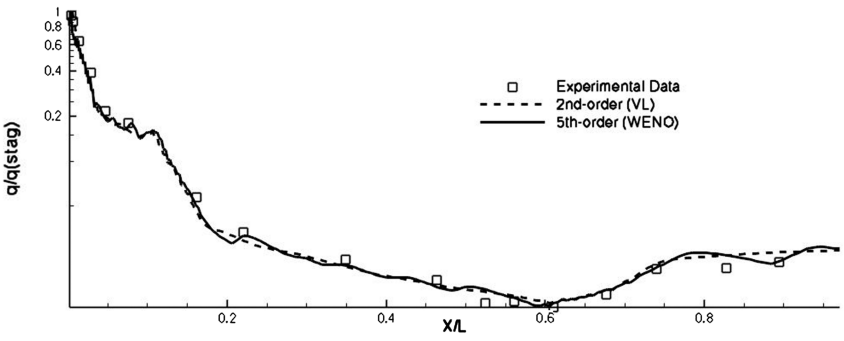

Fig. 11 Heat transfer distribution on the 256 × 128 grid for case 2.

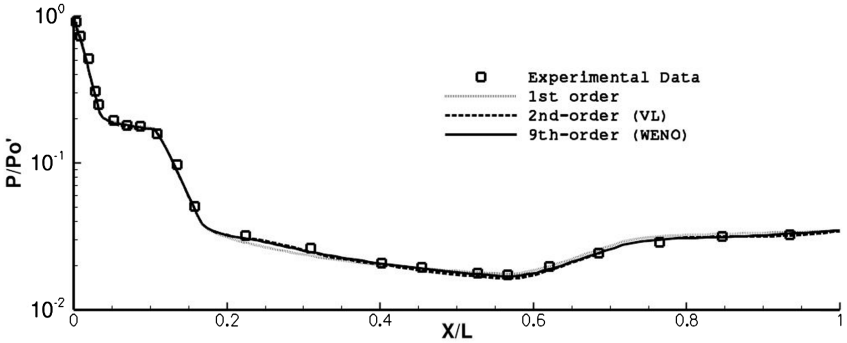

Fig. 12 Pressure distribution on the fine grid for case 3. The fifth-order MUSCL, second-order MUSCL (DD limiter), and fifth-order WENO scheme also gave very similar results; thus, they are not included in the graph.

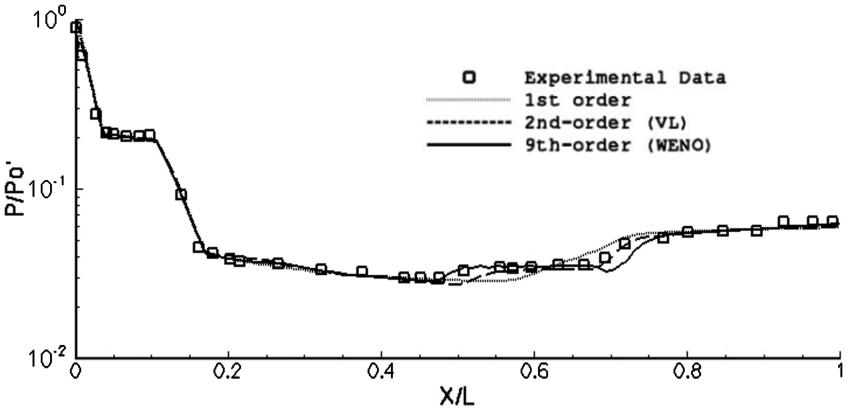

Fig. 13 Pressure distribution for case 4.

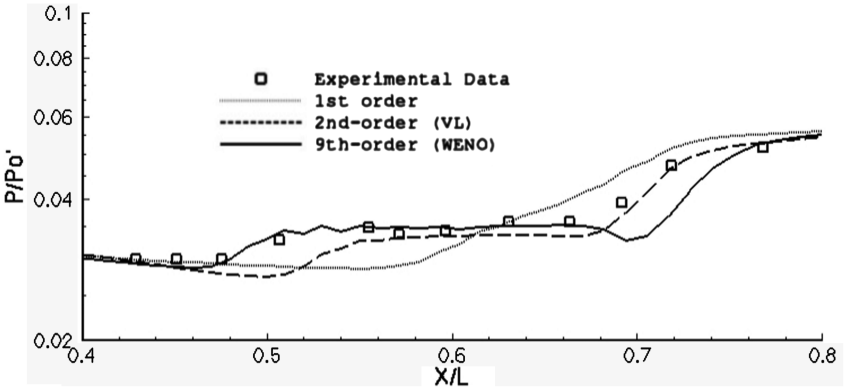

Fig. 14 Enlargement of pressure distribution at cylinder-flare transition for case 4.

Finally, the CPU requirement for the ninth-order WENO scheme compared to the second-order MUSCL increases by a factor of 2 and three on the coarse and fine grid resolutions, respectively. The fifth-order MUSCL requires only moderate CPU increase compared to the second-order MUSCL scheme.

Conclusions

Numerical experiments from the implementation of second-, fifth-, and ninth-order reconstruction schemes for hypersonic flows around the HB-2 hypersonic configuration were presented for freestream Mach numbers ranging from 5 to 17.8. The results show that WENO schemes can be unstable for Mach numbers above 10; however, they seem to be more accurate than second-order methods for Mach numbers less than 10. For the HB-2 geometry the fifth- and second-order MUSCL schemes give similar results and, additionally, the second-order MUSCL is more stable. Very similar results were obtained using the MUSCL scheme with two different limiters, with the DD limiter being numerically more robust across a range of Mach numbers.

Investigation of the behavior of these methods to high-enthalpy hypersonic flows featuring chemical reactions and ablation is underway and the results will be presented in a future paper.

Acknowledgments

The financial support from the U.K.'s Ministry of Defence/ Defence Science and Technology Laboratory is greatly acknowledged. S. Tissera and D. Drikakis would like to thank Vladimir Titarev for his comments on the manuscript as well as Andrew Mosedale for discussions on weighted essentially nonoscillatory schemes.

References

[1] Knight, D., and Longo, J., "Assessment of Aerothermodynamic Flight Prediction Tools for Shock Interactions," *48th AIAA Aerospace Sciences Meeting and Exhibit*, AIAA Paper 2010-1465, Orlando, FL, 4–7 January 2010.

[2] Gilchrist, A. R., and Williams, M. J., "Pressure Distributions and Forces on AGARD Models HB-1 and HB-2 at $M = 7.5$," Aeronautical Research Labs., Australian Defence Scientific Service, Aerodynamics Note 346, Feb. 1974.

[3] Jones, J. H., "Pressure Tests on the Standard Hypervelocity Ballistic Model HB-2 at Mach 1.5 to 5," von Karman Gas Dynamics Facility, TR AEDC-TDR-64-246, Arnold AFB, TN, 1964.

[4] Gray, J. D., "Summary Report on Aerodynamic Characteristics of Standard Models HB-1 and HB-2," von Karman Gas Dynamics Facility, TR AEDC-TDR-64-137, Arnold AFB, TN, 1964.

[5] Kharitonov, A., Kharitonov, A. M., Adamov, N. P., Brodetsky, M. D., Vasenyov, L. G., Mazhul, I. I., Zvegintsev, V. I., Paulat, J. C., Muylaert, J. M., and Kordulla, W., "Investigation of Aerogasdynamics of Reentry Vehicles in a New Hypersonic Wind Tunnel at ITAM," 44th AIAA Aerospace Sciences Meeting, AIAA Paper 2006-499, Reno, NV, Jan. 2006.

[6] Adamov, N. P., Vasenev, L. G., Zvegintsev, V. I., Mazhul, I. I., Nalivaichenko, D. G., Novikov, A. V., Kharitonov, A. M., and Shpak, S. I., "Characteristics of the AT-303 Hypersonic Wind Tunnel, Part 2. Aerodynamics of the HB-2 Reference Model," *Thermophysics and Aeromechanics*, Vol. 13, No. 2, 2006, pp. 157–171. doi:10.1134/S0869864306020016

[7] Kuchi-ishi, S., Watanbe, S., Nagai, S., Tsuda, S., Koyama, T., Hirabayashi, N., Sekine, H., and Hozumi, K., "Comparative Force/Heat Flux Measurement Between JAXA Hypersonic Test Facilities Using Standard Model HB-2 (Part 1: 1.27 m Hypersonic Wind Tunnel Results)," JAXA Research and Development, Rept. JAXA-RR-04-035E, March 2005.

[8] Kuchi-ishi, S., Watanbe, S., Nagai, S., Tsuda, S., Koyama, T., Hirabayashi, N., Sekine, H., and Hozumi, K., "Comparative Force/Heat Flux Measurement Between JAXA Hypersonic Test Facilities Using Standard Model HB-2 (Part 2: High Enthalpy Shock Tunnel Results)," JAXA Research and Development, Rept. JAXA-RR-05-030E, March 2006.

[9] Huang, J. C., Lin, H., and Yang, J. Y., "Implicit Preconditioned WENO Scheme for Steady Viscous Flow Computation," *Journal of Computational Physics*, Vol. 228, 2009, pp. 420–438. doi:10.1016/j.jcp.2008.09.017

[10] Birch, T. J., Prince, S. A., Ludlow, D. K., and Qin, N., "The Application of a Parabolized Navier–Stokes Solver to Some Hypersonic Flow Problems," AIAA/NAL-NASDA-ISAS International Space Planes and Hypersonic Systems and Technologies Conference, AIAA Paper 2001-1753, Kyoto, Japan, April 2001.

[11] van Leer, B., "Towards the Ultimate Conservative Difference Scheme V: A Second Order Sequel to Godunov's Method," *Journal of Computational Physics*, Vol. 32, 1979, pp. 101–136. doi:10.1016/0021-9991(79)90145-1

[12] Kim, K. H., and Kim, C., "Accurate, Efficient and Monotonic Numerical Methods for Multi-Dimensional Compressible Flows, Part II: Multi-Dimensional Limiting process," *Journal of Computational Physics*, Vol. 208, 2005, pp. 570–615. doi:10.1016/j.jcp.2005.02.022

[13] Harten, A., Engquist, B., Osher, S., and Chakravarthy, S. R., "Uniformly High Order Accurate Essentially Nonoscillatory Schemes III," *Journal of Computational Physics*, Vol. 71, 1987, pp. 231–303. doi:10.1016/0021-9991(87)90031-3

[14] Chiu, C. E., and Zhong, X., "Numerical Simulation of Transient Hypersonic Flow Using the Essentially Nonoscillatory Schemes," *AIAA Journal*, Vol. 34, No. 4, April 1996, pp. 655–661. doi:10.2514/3.13124

[15] Jiang, G. S., and Shu, C. W., "Efficient Implementation of Weighted ENO Schemes," *Journal of Computational Physics*, Vol. 126, 1996, pp. 202–228. doi:10.1006/jcph.1996.0130

[16] Wolf, W. R., and Azevedo, J. L. F., "Supersonic and Hypersonic Flow Computations Using Higher-Order Non-Oscillatory Schemes," AIAA Paper 2006-3169, June 2006.

[17] Kara, K., Balakumar, P., and Kandil, O. A., "Effects of Nose Bluntness on Stability of Hypersonic Boundary Layers over a Blunt Cone," AIAA Paper 2007-4492, June 2007.

[18] Oliveira, M. L., Xie, P., Su, J., and Liu, C., "Modified Weighted Compact Scheme for Shock-Boundary Layer Interaction and Double Cone," AIAA Paper 2008-755, Jan. 2008.

[19] Kara, K., Balakumar, P., and Kandil, O. A., "Receptivity of Hypersonic Boundary Layers due to Acoustic Disturbances over Blunt Cone," 45th AIAA Aerospace Sciences Meeting, AIAA Paper 2007-947, Reno, NV, Jan. 2007.

[20] Liu, X. D., Osher, S., and Chan, T., "Weighted Essentially Non-Oscillatory Scheme," *Journal of Computational Physics*, Vol. 110, 1994, pp. 200–212. doi:10.1006/jcph.1994.1017

[21] Yang, J. Y., Perng, R. H., and Yen, Y. C., "Implicit Weighted Essentially Nonoscillatory Schemes for the Compressible Navier–Stokes Equations," *AIAA Journal*, Vol. 39, No. 11, 2001, pp. 2082–2090. doi:10.2514/2.1231

[22] Balsara, D. S., and Shu, C. W., "Monotonicity Preserving Weighted Essentially Non-Ooscillatory Schemes with Increasingly High Order of Accuracy," *Journal of Computational Physics*, Vol. 160, 2000, pp. 405–452. doi:10.1006/jcph.2000.6443

[23] Titarev, V. A., and Toro, E. F., "Finite Volume WENO Schemes for Three-Dimensional Conservation Laws," *Journal of Computational Physics*, Vol. 201, 2004, pp. 238–260. doi:10.1016/j.jcp.2004.05.015

[24] Henrick, A. K., Aslam, T. D., and Powers, J. M., "Mapped Weighted Essentially Nonoscillatory Schemes: Achieving Optimal Order Near Critical Points," *Journal of Computational Physics*, Vol. 207, 2005, pp. 542–567. doi:10.1016/j.jcp.2005.01.023

[25] Borges, R., Carmona, M., Costa, B., and Don, W. S., "An Improved Weighted Essentially Non-Oscillatory Scheme for Hyperbolic Conservation Laws," *Journal of Computational Physics*, Vol. 227, 2008, pp. 3191–3211. doi:10.1016/j.jcp.2007.11.038

[26] Drikakis, D., and Tsangaris, S., "Real Gas Effects for Compressible Nozzle Flow," *Journal of Fluids Engineering*, Vol. 115, 1993, pp. 115–120. doi:10.1115/1.2910092

[27] Drikakis, D., and Tsangaris, S., "On the Accuracy and Efficiency of CFD Methods in Real Gas Hypersonics," *International Journal for Numerical Methods in Fluids*, Vol. 16, 1993, pp. 759–775. doi:10.1002/fld.1650160902

[28] Drikakis, D., "Advances in Turbulent Flow Computations Using High-Resolution Methods," *Progress in Aerospace Sciences*, Vol. 39, 2003, pp. 405–424. doi:10.1016/S0376-0421(03)00075-7

[29] Bagabir, A., and Drikakis, D., "Numerical Experiments Using High-Resolution Schemes for Unsteady, Inviscid, Compressible Flows," *Computer Methods in Applied Mechanics and Engineering*, Vol. 193, March 2004, pp. 4675–4705. doi:10.1016/j.cma.2004.03.012

[30] Zółtak, J., and Drikakis, D., "Hybrid Upwind Methods for the Simulation of Unsteady Shock-Wave Diffraction over a Cylinder," *Computer Methods in Applied Mechanics and Engineering*, Vol. 162, Oct. 1998, pp. 165–185. doi:10.1016/S0045-7825(97)00342-3

[31] Toro, E. F., *Riemann Solvers and Numerical Methods for Fluid Dynamics a Practical Introduction*, 2nd ed., Springer–Verlag, Berlin, 1999, pp. 1–624.

[32] Ivings, M. J., Causon, D. M., and Toro, E. F., "On Riemann Solvers for Compressible Liquids," *International Journal for Numerical Methods in Fluids*, Vol. 28, No. 3, 1998, pp. 395–418. doi:10.1002/(SICI)1097-0363(19980915)28:3<395::AID-FLD718>3.0.CO;2-S

[33] Drikakis, D., and Tsangaris, S., "On the Solution of the Compressible Navier–Stokes Equations Using Improved Flux Vector Splitting Methods," *Applied Mathematical Modelling*, Vol. 17, 1993, pp. 282–297. doi:10.1016/0307-904X(93)90054-K

[34] Drikakis, D., and Rider, W., *High-Resolution Methods for Incompressible and Low-Speed Flows*, Springer–Verlag, Berlin, 2005, pp. 1–622.

G. Palmer
Associate Editor